REPORT DOCUMENTATION PAGE

Form Approved
OMB No. 0704-0188

1. REPORT DATE *(DD-MM-YYYY)*	2. REPORT TYPE	3. DATES COVERED *(From - To)*
04/01/2009	Final	01/01/05 – 12/31/08

4. TITLE AND SUBTITLE

Nucleation and Microalloying for Control of Nano-Structure Refinement

5a. CONTRACT NUMBER

5b. GRANT NUMBER
FA 9550-05-1-0110

5c. PROGRAM ELEMENT NUMBER

6. AUTHOR(S)

Dr. Kenneth F. Kelton

Dr. William E. Buhro

5d. PROJECT NUMBER

5e. TASK NUMBER

5f. WORK UNIT NUMBER

7. PERFORMING ORGANIZATION NAME(S) AND ADDRESS(ES)

Washington University
Campus Box 1054
One Brookings Drive
St. Louis, MO 63130

8. PERFORMING ORGANIZATION REPORT NUMBER

9. SPONSORING / MONITORING AGENCY NAME(S) AND ADDRESS(ES)

UFOSR/PK4
USAF/AFRL
AF Office of Scientific Research
801 N. Randolph St., Room 732
Arlington, VA 22203-1977

10. SPONSOR/MONITOR'S ACRONYM(S)

11. SPONSOR/MONITOR'S REPORT
AFRL-OSR-VA-TR-2013-0904

12. DISTRIBUTION / AVAILABILITY STATEMENT

13. SUPPLEMENTARY NOTES

14. ABSTRACT

Kinetic transformation studies in rapidly-quenched $Al_{88}Y_7Fe_5$ alloys, under previous AFOSR support raised concern that they were not amorphous. The substitution of 0.5 – 2.0 at.% of the Al by Ti, Zr, and V produced glasses with improved stability against crystallization. Under funding from this grant we demonstrated that the $Al_{88}Y_7Fe_5$ alloys are amorphous, but this is masked in devitrification studies because of the extremely high nucleation rates and low growth rates of α-Al. We have explored further the influence of microalloying by systematically adding small additions of each element in the 3d transition metal series. Primary crystallization is to α-Al for the early (Ti, V, Cr) and late (Co, Ni, Cu) 3d transition metals. For Mn and Fe, an intermetallic phase forms first, which is closer in composition to the original glass. Kinetic calorimetric and microstructural studies of devitrification show that the microadditions raise the nucleation barrier of the crystal phase and decrease the rate of diffusion-limited growth. Scanning probe fluctuation microscopy studies show that the microadditions change the medium-range order. Complementary atom probe tomography studies, supported by our NSF grant (DMR-0606065), show that the Ti microaddition suppresses a nanoscale phase separation in the $Al_{88}Y_7Fe_5$ glass.

15. SUBJECT TERMS

16. SECURITY CLASSIFICATION OF:			17. LIMITATION OF ABSTRACT	18. NUMBER OF PAGES	19a. NAME OF RESPONSIBLE PERSON
a. REPORT	b. ABSTRACT	c. THIS PAGE			19b. TELEPHONE NUMBER *(include area code)*

Final Technical Report

Nucleation and Microalloying for Control of Nano-Structure Refinement

Grant
AFOSR FA 9550-05-1-0110

Prepared for
AIR FORCE OFFICE OF SCIENTIFIC RESEARCH

For the Period
01/01/05 – 12/31/08

Submitted by:

Kenneth F. Kelton, Principle Investigator
William E. Buhro, Co-Principle Investigator

Departments of Physics and Chemistry
Washington University, St. Louis, Missouri 63130

Abstract

Kinetic transformation studies in rapidly-quenched $Al_{88}Y_7Fe_5$ alloys, under previous AFOSR support raised concern that they were not amorphous. The substitution of 0.5 – 2.0 at.% of the Al by Ti, Zr, and V produced glasses with improved stability against crystallization. Under funding from this grant we demonstrated that the $Al_{88}Y_7Fe_5$ alloys are amorphous, but this is masked in devitrification studies because of the extremely high nucleation rates and low growth rates of α-Al. We have explored further the influence of microalloying by systematically adding small additions of each element in the 3d transition metal series. Primary crystallization is to α-Al for the early (Ti, V, Cr) and late (Co, Ni, Cu) 3d transition metals. For Mn and Fe, an intermetallic phase forms first, which is closer in composition to the original glass. Kinetic calorimetric and microstructural studies of devitrification show that the microadditions raise the nucleation barrier of the crystal phase and decrease the rate of diffusion-limited growth. Scanning probe fluctuation microscopy studies show that the microadditions change the medium-range order. Complementary atom probe tomography studies, supported by our NSF grant (DMR-0606065), show that the Ti microaddition suppresses a nanoscale phase separation in the $Al_{88}Y_7Fe_5$ glass.

Executive Summary

The Al-3d transition metal – rare earth (Al-TM-RE) glasses, containing greater than 80 at.% Al are interesting for potential structural applications, showing a high strength-to-weight and good corrosion resistance. Further, many Al-TM-RE glasses crystallize to amorphous/nanocrystal composites that often have even superior properties to those of the original glasses. Our investigations made under previous AFOSR support of the crystallization of well-studied rapidly-quenched $Al_{88}Y_7Fe_5$ glasses raised a concern that they might not be amorphous, but completely transformed amorphous/nanocrystal composites. They showed no glass transition in nonisothermal differential scanning calorimetry (DSC) studies and their behavior during isothermal DSC annealing was more typical of coarsening rather than a nucleation and growth transformation. We discovered that the substitution of 0.5 – 2.0 at.% of the Al by Ti, Zr, and V produced glasses with improved stability against crystallization. However, the mechanism by which microalloying gave these improvements was unclear; it was not as simple as internal gettering of oxygen as is often the case.

The goal of the research funded under AFOSR FA 9550-05-1-0110 was to determine quantitatively whether rapidly-quenched $Al_{88}Y_7Fe_5$ is a glass, to uncover the reasons for nanocrystal formation, and to develop a better understanding of the role of the transition metal microadditions in giving improved glass formation and stability. The proposed experimental program included (i) DSC and electrical resistivity studies of the isothermal transformation kinetics in $Al_{88}Y_7Fe_5$ alloys to discern the phase structure , (ii) investigations of the effectiveness of other 3d transition metal microadditions on glass formation and stability and (iii) fluctuation electron microscopy studies of rapidly-quenched $Al_{88}Y_7Fe_5$ and $Al_{87.5}Y_7Fe_5Ti_{0.5}$ alloys to determine whether the improved glass formability and stability is due to changes in the medium range order.

Our investigation has been successful. A quantitative analysis of calorimetric, resistivity and grain counting measurements as a function of isothermal annealing, demonstrates that rapidly quenched $Al_{88}Y_7Fe_5$ alloys are indeed amorphous. Their transformation is dominated by an extremely rapid nucleation rate followed by very slow diffusion-limited growth, likely due to rejection of the Y. Calorimetric and microstructural studies indicate that all 3d transition metal microadditions raise the nucleation barrier for the α-Al phase and increase the role of long-range diffusion. Fluctuation electron microscopy (SP-FEM), of samples made with and without Ti, show that the microaddition induces a change in the medium range order; the variance in samples made with Ti is lower than in samples without Ti. A comparison with atom probe tomography measurements performed by us under NSF support shows that this is due to a suppression of nanoscale phase separation in the $Al_{88}Y_7Fe_5$ glass by the introduction of Ti.

These results provide valuable insight into the role of microadditions in Al-based glass formation, and the mechanism of nanocrystallization. This information will be valuable in designing more stable glasses and developing methods for microstructural optimization.

I. Introduction and Motivation

The Aluminum-Rare Earth-3d Transition Metal (Al-RE-TM) glasses, containing greater than 80 at.% Al, are of significant interest for civilian and military aerospace applications. They have a high strength, sometimes exceeding 1000 MPa [1, 2], low densities, near 3.3 g/cm^3 [3], good corrosion resistance [4] and are produced from relatively low cost materials.

Many of the Al-RE-TM glasses crystallize (devitrify) to form amorphous/nanocrystal composites, often with α-Al as the primary crystallizing phase. These nano-composites have even superior properties to those of the original glasses, with reported tensile strengths as high as 1200-1500 MPa [5]. In addition the hardness, Young's modulus and fracture elongation all exhibit significant increases with nanocrystal formation [2]. The enhanced mechanical properties are thought to arise from the high solute content in the amorphous matrix [6], and interaction between the dispersed Al nanocrystals and shear bands that develop upon deformation of the amorphous matrix [2]. The dispersed α-Al nanocrystals also provide increased ductility.

Our work has focused on the $Al_{88}Y_7Fe_5$ (Al-Y-Fe) glass. The nanostructures observed after devitrification, with grain densities ranging from $10^{20}/m^3$ to $10^{23}/m^3$ and grain diameters between 5 and 20 nm, suggest extremely high nucleation rates and slow growth velocities. Such nanocrystal formation is not limited to the Al-based glasses, but is common in all of the glass systems, including the Zr-based bulk metallic glasses, and the Mg- and Fe-based glasses. In the Zr-based glasses, the nanoscale grains are often icosahedral quasicrystals, forming because of the significant short-range icosahedral order in the glass. However, our x-ray diffraction studies have shown that the Al-based glasses do not appear to have strong icosahedral order and devitrify to non-quasicrystal phases, such as α-Al or complex intermetallics. A different explanation is, therefore, required for the low nucleation barrier. Further, it is unclear whether rapidly quenched Al-Y-Fe is even a glass. Isothermal differential scanning calorimetry (DSC) studies do not show the expected peak for a nucleation and growth transformation, but are more reminiscent of coarsening. This suggests that the rapidly quenched alloys could be essentially completely transformed nanocrystal/amorphous composites instead of metallic glasses.

It has been shown that glass formation and stability is often improved dramatically by small changes in the alloy composition and by the addition of small amounts of certain elements (microalloying). Our research has demonstrated that microalloying with 3d transition metals dramatically improves the glass formability and crystallization behavior in the rapidly-quenched Al-Y-Fe alloys [7]. We also have used microalloying to develop a new metallic glass that has among the largest supercooled liquid regions on record for Al-based glasses [8]. The success of microalloying in improving glass formation and enhancing glass stability, particularly in Al-based glasses, makes it important to develop a better understanding of the underlying mechanism.

Finally, while bulk metallic glasses have been discovered in many multi-component Zr- and Mg-based alloys, allowing glass formation and fabrication at slow cooling rates, essentially all of the Al-RE-TM glasses require that the liquids be quenched at rates of 10^5-10^6 °C/s for their formation. This yields thin ribbons that are difficult to process, limiting their technological usefulness. There are some reports of aluminum-based glasses produced by the consolidation of amorphous powders that show significant compressive strength, but they have not yet proven useful as technological materials.

With this background and supported by AFOSR Contract FA 9550-05-1-0110, we proposed a three-year research program to:

- carry out quantitative studies of the nucleation and crystallization kinetics in select Al-TM-RE glasses using DSC and electrical resistivity measurements;
- measure the particle densities of α-Al, the primary crystallizing phase, to determine whether the Al-Y-Fe was a glass or a transformed nanocrystal/amorphous composite;
- study the structures of Al-TM-RE glasses containing small amounts of 3d transition metals, like Ti, using a new technique, fluctuation TEM (FTEM);
- search for a bulk-glass-forming composition in the Al-Y-Fe-V system.

We have completed these studies, giving the following results.

- Rapidly-quenched Al-Fe-Y alloys are indeed glasses.
- They have a low barrier to the nucleation of the α-Al phase, explaining the high grain density and are strongly diffusion-controlled in growth, explaining the small grain sizes.
- Glass formation and stability is very sensitive to the precise alloy chemical composition.
- Glass formation, glass stability, and the primary crystallizing phase are sensitive to the 3d transition metal microalloying element used.
- Fluctuation electron microscopy can be used to identify changes in medium-range ordering with microaddition, but only if great care is taken in sample preparation and the measurement technique.

The results and conclusions of the investigations partially supported by AFOSR are provided in this final report. These studies have provided new information on nanocrystal formation and coupled phase transformations in metallic glasses. They also suggest methods for improved glass formation and microstructural refinement by the

selection of appropriate miocroadditions and the development of well-designed post-quenching annealing cycles.

II. Background

Before presenting and discussing the key results from the research sponsored by AFOSR Contract FA 9550-05-1-0110, it is useful to present some background material.

Formation and Structure of Al-based Glasses

Inoue *et al.* [9, 10] and He *et al.* [11] first reported glass formation in alloys containing greater than 80 at.% Al. Many examples have now been discovered in both binary (Al-RE) and ternary (Al-RE-TM) alloys. To date these are marginal glass formers; no Al-based bulk metallic glass is known, although cast glasses with a thickness approaching 1 mm have been reported. Surprisingly, these alloys lack deep eutectics, commonly correlated with easy glass formation; they appear to form from the large size differences and negative heats of mixing of the constituent elements. Glass formation occurs over a limited range; as will be discussed in §IV, our work shows it can degrade significantly with as little as a 0.5 at.% change in the transition metal concentration.

The reasons for glass formation in these Al-alloys and their relation to the glass structures are unclear. The importance of the concentration and size of solute atoms has long been recognized [12], presumably arising from tensile and compressive strains produced by the introduction of small (S) and large (L) atoms in the solvent matrix. Interactions between these stress fields are argued to lead to the formation of stable regions of short-range order that stabilize glass formation [13]. Further, the criteria for bulk metallic glass formation that emerge from an examination of the local strain required to produce a topological instability are strikingly similar to those experimentally determined: (i) alloys with a large number of elements, (ii) increased size ratio of the constituent elements, (ii) increased interactions between the small and large atoms and (iv) repulsive interactions between small atoms [14].

Poon *et al.* argue from the concentrations of the Al-based glasses, with the major component (60-70 at.%) mid-sized atoms (M), followed by a lower concentration of the S atoms (20-30 at.%), and the least concentration (10 at.% or less) of the L atoms [15]. The heats of mixing are large and negative between the S-L pairs and in many cases are larger than with the solvent (M) atoms. The L-S atoms are argued to form a network that enhances the stability of the supercooled liquid, favoring glass formation. Supporting this notion, a correlation between the maximum thicknesses of glass forming ribbons with decreasing heats of mixing with the TM (from Ni to Co to Fe), was noticed in $Al_{87}TM_6Gd_6$ alloys. If the concentration of L atoms is too high they will tend to cluster and reduce their interaction with the other atoms, preventing network formation.

Metallic glasses contain not only short-range order, but also often a significant amount of medium range order. To account for both, Miracle has proposed a model that close-packs solute-centered atomic clusters into crystal lattices (fcc or hcp) [16]. This is not a

periodic model for a glass; internal strains will quickly degrade the coherence length of the order. However, it provides one consistent way of taking local cluster-cluster interactions into account. In addition to the solvent sites (denoted as Ω) and the substitutional solute sites (α), there are two additional topologically distinct interstitial solute sites in the model, the β sites in the cluster-octahedral interstices and the γ sites located in the cluster-tetrahedral interstices. The α atoms are the largest solute atoms followed in turn by the β and γ solute atoms. By examining cases of different coordination numbers for efficient packing, good agreement was obtained for the concentrations and sizes of known glass formers. The β and γ sites are vacant in the Al-RE binary glasses; the structures of the ternary Al-RE-TM glasses have not been reported.

A. Nanocrystallization

Many metallic glasses, including the Al-based ones, devitrify to an amorphous/nanocrystal composite (nano-composite). The high grain densities ($10^{20}/m^3$ to $10^{23}/m^3$) and grain sizes of a few nm signal an extremely high nucleation rate and a low growth velocity. Grain growth is typically initially rapid, but abruptly slows down when the grain size exceeds a few nm; there is also little temperature dependence on the final grain sizes [17].

As mentioned earlier, the reasons for nanoscale crystallization remain unclear. The primary crystallizing phase is often α-Al, although the driving free energy is generally larger for other intermetallic phases [2], suggesting that pre-existing growth centers are present. This could indicate the growth of quenched-in nuclei [18], supported by evidence for nanoscale clusters in as-quenched glasses [19]. However, the steady-state nucleation rate would need to be unphysically large to generate the observed density of nuclei during the quench, due to the orders of magnitude depression of the nucleation rate during the quench from transient nucleation effects [20]. The observed saturation of the nucleation rate with increased annealing time could signal a heterogeneous mechanism, although the required density of catalytic sites also would be unrealistically high. Other mechanism that have been proposed include short-range order in the glass that is incompatible with that of the competing crystal phase [21-23], heterogeneous precipitate formation [24], and phase separation [25].

Coupled processes are important for the formation, stability, and microstructural refinement in many metallic and silicate glasses. Coupled phase transformations such as phase separation on a fine scale [26, 27] and the precipitation of phases that effectively catalyze crystal nucleation [28, 29], lead to the formation of nanocrystal/amorphous composites during the crystallization of some metallic glasses. Coupling goes beyond such straightforward examples, however. For example, long-range diffusion generally plays an important role in the nucleation and growth of crystal phases in the multicomponent glasses of current interest. Nucleation cannot be quantitatively modeled by the classical theory in this case, since the stochastic fluxes of interfacial attachment and long-range diffusion are coupled [30], which may lead to nanocrystal formation [31].

Structural [32] and chemical [33] ordering can also greatly influence nucleation, through a coupling of different order parameters. Recent structural and nucleation studies on undercooled Ti-Zr-Ni liquids, for example, have shown that growing icosahedral order in the liquid catalyzes the nucleation of a metastable icosahedral quasicrystal phase (i-phase). In addition to confirming a half-century old hypothesis of the origin of the nucleation barrier in metallic liquids [34], these results demonstrate that the local structures in metallic liquids can dictate the phases that form, blurring the distinction between homogeneous and heterogeneous nucleation in such cases. It is becoming increasingly clear that such couplings between the nucleation barrier and other processes or phase transitions is much more common than previously thought.

B. Microalloying

Often, glass formation and crystallization can be profoundly influenced by the addition of small amounts of particular elements (microalloying) at levels of a few percent or less. For example, the addition of 0.2-3.0 at.% of Fe, Co, Ni, Nb, Si, Co or B to Ce-Al-Cu alloys can increase the maximum diameter of cast glasses from 2 mm to 10 mm [35]. Other examples are found in Zr-based [36], Cu-based [37, 38] and Fe-based [39] glasses. Good reviews of microalloying in glasses are found in Ref. [40] and [41]. We have also discovered improved glass formation and stability with microalloying in Al-based glasses [7, 8].

The mechanism by which microalloying improves glass formation is unclear. It must either increase the stability of the liquid phase, or make nucleation and growth of the crystal phase more difficult. Often the microaddition decreases the nucleation rate of competing crystal phases by scavenging oxygen that would otherwise form heterogeneously nucleating oxide particles. However, our previous research has ruled this out for the Al-based glasses of interest to this AFOSR sponsored research [7].

In some Zr-based glasses it is well known that crystallization to the icosahedral quasicrystal phase is enhanced by the addition of O [42, 43], noble elements such as Ag, Au, Pd and Pt [44] and the transition metals Nb, Ta, V [45] and Ti [46, 47]. In these cases, the negative heats of mixing of the microadditions with Zr likely form strong icosahedral short-range order in the liquid/glass. Following Frank's hypothesis [34] the enhanced icosahedral order in these liquids raises the barrier for the formation of the crystal phases during the quench, enhancing glass formation. Microadditions need not induce only icosahedral order to influence glass formation and crystallization, however. They must only enhance a short-range order in the liquid or glass that is incompatible with that of the crystallizing phase. Our work suggests that this is the case in the Al-based glasses.

III. Sample Preparation and Characterization

These studies focused entirely on $Al_{87.5}Y_7Fe_5TM_x$ alloys, where TM stands for a 3d transition metal. Sample ingots were prepared by arc-melting the elemental components

on a water-cooled copper hearth, which was first evacuated to $3x10^{-2}$ Torr and backfilled with high-purity Ar gas (99.999%). A Ti-getter located close to the samples was melted prior to arc-melting to further remove oxygen from the chamber. The samples were flipped and re-melted several times to ensure a homogeneous composition; the duration of each melt cycle was approximately one minute. Amorphous ribbons were prepared by melting the ingots using rf-induction heating to 1100-1150°C (well above the liquidus temperature) in a graphite crucible under an Ar atmosphere, and rapidly quenching the liquid onto a copper wheel rotating at 3800 m/min. The quenched ribbons were continuous for 10-250 cm and had an average cross section of 1-2 mm by 20-30 μm.

The as-quenched ribbons were characterized by x-ray diffraction (Rigaku, Cu K_α, λ = 1.54Å radiation), DSC (Perkin-Elmer, model *DSC 7*), and electrical resistivity measurements. *In-situ* resistivity measurements were made using a four-probe technique, with a Fluke 8505A digital volt meter and a computer controlled switching circuit to reduce thermocouple effects [48]. For these measurements, approximately 3cm long ribbons were placed in an insulating MACOR® holder that was inserted into a furnace constructed from a large copper cylinder (~1 kg). The samples were initially held in a water-cooled copper block; they were inserted into the furnace after it had stabilized at the desired temperature. All resistivity measurements were made in Ti-gettered high-purity (99.995%) argon atmosphere. A thermocouple was used to monitor sample temperature; the thermal stability was typically ±.1% over 80 hours.

The sample microstructures of the as-quenched and annealed samples were examined using a JEOL 2000FX transmission electron microscope. Scanning probe fluctuation electron microscope (SP-FEM) studies were made using a JEOL JEM-2100F scanning field emission transmission electron microscope. The TEM specimens were prepared by ion milling with liquid nitrogen cooling (GATAN, model 600) and by electrochemical jet thinning. Since ion milling induced damage that completely obscured features of interest in the SP-FEM studies, all of those samples were prepared by chemical jet thinning.

For the TEM studies of annealed glasses, the ribbons were wrapped in aluminum foil and completely immersed in a lead-tin solder bath. The high thermal conductivity of the foil allowed the samples to reach the annealing temperature quickly; the large thermal mass of the bath enabled the temperature to remain stable over the duration of the anneal.

NSF-sponsored studies (DMR-0606065) - Complementary x-ray synchrotron and three dimensional atom probe tomography (3DAP) measurements were made, which were supported by my NSF grant (DMR-0606065). The high-energy synchrotron x-ray diffraction measurements (100 keV, wavelength $\lambda = 0.1247$ Å) were made on beam line 6-ID-D in the MUCAT Sector at the Advanced Photon Source, Argonne National Laboratory. A MAR 345 image plate area detector allowed data to be collected over a wide range of scattering angle, $q = 0.5–14$ Å^{-1}. The 3DAP measurements on as-quenched ribbons were made in collaboration with Mike Miller at Oak Ridge National Laboratory, using the Imago Scientific Instruments Local Electrode Atom Probe (LEAP). The instrument time was obtained under the SHaRE program. In most cases the sample tips for the 3DAP measurements were made by electrolytic pulse polishing. The ribbons

were first cut into 7- 10 mm long sections and the tops and bottoms of the ribbons were lightly sanded with 1000 grit sandpaper. The samples were further sanded to produce an approximately square cross-section; samples with elliptical cross sections produce data that cannot be reconstructed reliably. An electrolytic pulse polishing technique was used to prepare the samples to a suitable size. For this step a thin film of the etchant was held suspended by a metal loop and an AC or DC current was applied. The sample was slowly moved up and down through this film while the voltage was pulsed. Etching only occurred where the etchant film contacted the sample, creating a "neck" in the material. For optimal conditions the polishing thinned the necked region until it broke, leaving a point that was only ~ 200 nm in diameter. A few pulses at the break were usually sufficient to create a tip that was sufficiently uniform to be suitable for 3DAP studies. Once prepared, the samples were quickly loaded into the 3DAP vacuum chamber to minimize oxidation.

IV. Research Results and Discussion

DSC studies of rapidly-quenched $Al_{88}Y_7Fe_5$ alloys reveal no glass transition and show isothermal transformation kinetics that suggest coarsening of α-Al grains in a transformed nanocrystal/amorphous composite material [7]. We have shown recently that the substitution of as little as 0.5 at.% of Ti for the Al yields an amorphous metal on quenching with an enhanced stability [7]. In this section we report the results of a systematic survey of the effects of microalloying with other 3d transitions metals (TM). Most of the microalloyed samples show amorphous diffraction patterns, well-defined glass transitions, a devitrification temperature that is 20 to 40 °C higher than the transformation temperature in the alloy made without TM substitution, and a large supercooled region, ΔT_x, over 40°C in some cases. The crystallization (devitrification) pathways, liquidus temperatures, and primary devitrification products are all extremely sensitive to composition and processing conditions, however. None of the common predictive parameters for glass formation explain the role of the microadditions. Instead, microalloying appears to order the glass, raising the nucleation barrier for α-Al and decreasing the atomic mobility for diffusion-controlled crystallization.

A. Are Rapidly-Quenched $Al_{88}Y_7Fe_5$ Alloys Amorphous?

As illustrated in Fig. 1.a, rapidly quenched ribbons of $Al_{88}Y_7Fe_5$ show the featureless bright field images expected for an amorphous material. In agreement, the x-ray and TEM diffraction patterns show the broad features of a glass with no suggestion of Bragg peaks. As shown in Fig. 1.b – 1.d, annealing of the glass causes the precipitation of nanocrystals of α-Al. The number of crystals increases with annealing time, but the grains show little growth.

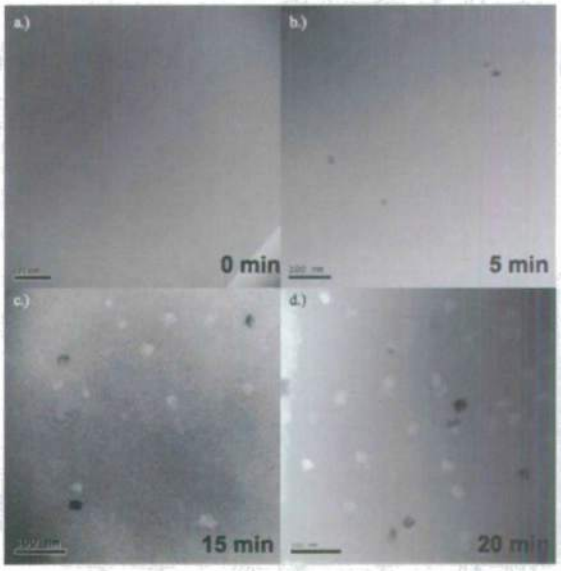

Figure 1 - A series of bright-field TEM images of $Al_{88}Y_7Fe_5$ showing the microstructure development of the primary transformation (α-Al) upon annealing at 250°C at (a) 0 min (as-quenched), (b) 5 min, (c) 15min and (d) 20min. The growth morphology is roughly spherical.

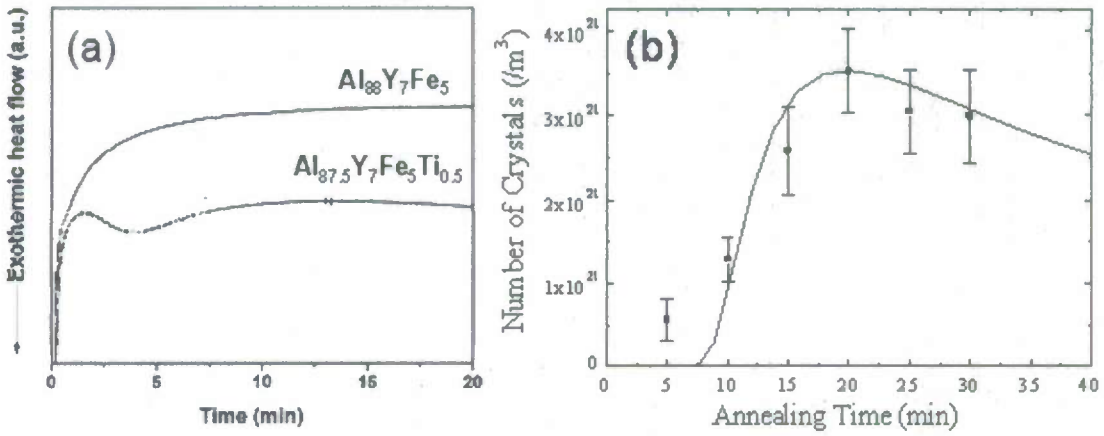

Figure 2 – (a) DSC traces for isothermal annealing of rapidly-quenched samples of $Al_{88}Y_7Fe_5$ and $Al_{87.5}Y_7Fe_5Ti_{0.5}$. (b) Crystal density determined from bright-field TEM image studies as a function of annealing time (250°C) for $Al_{88}Y_7Fe_5$. The line serves as a guide to the eye.

While the transformation sequence in Fig. 1 is consistent with a nucleation and growth based devitrification of the glass, the expected peak in heat released as measured in isothermal DSC studies, is not observed (Fig. 2.a). The DSC trace obtained is typically taken to indicate grain coarsening [49, 50], suggesting that the sample might not be a glass, but a transformed nano-composite. Our calculations, based on a coupled-flux model for diffusion-limited nucleation [30, 51] and growth, however, indicate that the monotonically decreasing DSC trace could also be consistent with the diffusion-limited growth of a high density of nuclei [52]. Figure 2.b shows that the number density of α-

Al crystals (the primary crystallizing phase) increases approximately linearly with time during isothermal annealing treatments, consistent with a steady-state nucleation rate and in agreement with these calculations. The subsequent decrease in crystallite number density suggests coarsening, which is likely occurring simultaneously with nucleation and growth.

Coarsening of an extremely fine nanostructured material could also produce similar results to those shown in Fig. 2.b. The grains in the as-cast samples might be too small to observe in TEM. As they coarsen with annealing, they would grow to visible size and thus appear to increase in number, mimicking nucleation. While, HREM studies showed no evidence of crystal grains in the as-quenched alloys, kinetic measurements were used to confirm this. Assume a conservative lower bound of ~ 2 nm for the radius of a crystal that could not be resolved in a bright field image. In a coarsening dominated regime, larger crystallites grow at the expense of smaller ones. The thermodynamic driving force for this is the size-dependent chemical potential of the crystallites, which changes the equilibrium solubility of a crystallite of finite radius from that of a particle of infinite radius according to the Gibbs-Thompson equation. The classic treatment of coarsening is due to Lifshitz and Slyozov, and Wagner (LSW) [53, 54]. It is valid for the late stages of coarsening in cases where the volume fraction of the minority phase is small and unchanging. LSW theory predicts the following distribution of particles as a function of radius R, where $z = R/\overline{R}(t)$,

$$g(z) = \left(\frac{3^4 \, e^{z^2} \exp\left(-1/\left(1 - \frac{2}{3} z \right) \right)}{2^{5/3} \left(z+3 \right)^{7/3} \left(3/2 - z \right)^{11/3}} \right) \quad if \quad 0 \le z \; 3/2$$

$$= 0 \quad otherwise \qquad , \qquad (1)$$

where, $\overline{R}(t)$ is the time-dependent average radius. Average quantities, $\langle x \rangle$, are calculated from the droplet distribution as

$$\langle x(t) \rangle = \frac{\int dr \; g(r,t) \, x(r,t)}{\int dr \; g(r,t)} . \qquad (2)$$

Because the average radius increases with time, the singly-peaked distribution shifts and broadens with time. To illustrate this, calculated distributions and an assumed observable limit in TEM of 2.0 nm are shown in Fig. 3. If the entire distribution lies below the observable limit no crystallites will be observed. As the distribution evolves, new particles will grow into view, appearing to be a nucleation and growth process, hiding the actual coarsening character of the transformation.

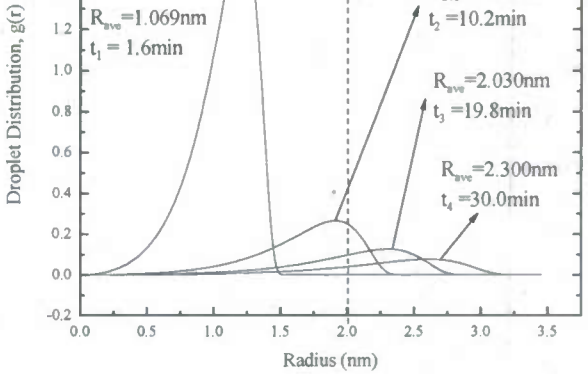

Figure 3 - Evolution of a sample droplet distribution given by LSW coarsening theory. As the droplet distribution evolves in time, the average radius increases and the distribution spreads. For this example (TEM visualization cutoff of 2.0nm) the distribution initially lies completely below the cutoff and the true character of the transformation is hidden.

For diffusion-limited coarsening, the time-dependent average radius, $\langle r(t) \rangle$, increases as

$$\langle r(t) \rangle = \left(\langle r(0) \rangle^3 + K(T)t \right)^{1/3}, \tag{3}$$

where $\langle r(0) \rangle$ is the average radius at $t = 0$ and $K(T)$ is a temperature-dependent rate constant. This typically taken to have an Arrhenius-type scaling with temperature,

$$K(T) = K_o \exp\left(-\frac{Q}{k_B T} \right), \tag{4}$$

where T is the temperature in absolute units, k_B is Boltzman's constant, Q is the activation energy and K_o is a constant. Following Chen and Spaepen [49, 50], the activation energy can be determined by measuring the shift in peak temperature of the primary crystallization peak (to α-Al in this case) as a function of scan rate (dT/dt) in nonisothermal DSC studies, giving $Q = 2.62 \pm 0.03$ eV. They also show argue that the rate of heat released in DSC isothermal scans due to coarsening is

$$P = \frac{dH}{dt} = \left(\frac{H_o r_o}{3} \right) \frac{K(T)}{\left[r_o^3 + \dfrac{k_B T^2 \, K(T)}{Q \left(dT / dt \right)} \right]^{4/3}}, \tag{5}$$

where H_o is the total enthalpy arising from the large surface to volume ratio of the non-coarsened material. By measuring P at the same temperature for different scan rates it is possible to determine all of the unknown parameters and to calculate $<r(t)>$ from eq. (3). The calculated value for $<r>$ is much less than the measured one (Fig. 2) indicating that the process is not one of coarsening but of nucleation and growth. The slow decrease in the number of grains observed in Fig. 1 after approximately 20 minutes of annealing time, however, is evidence for coarsening in the late stages of the transformation.

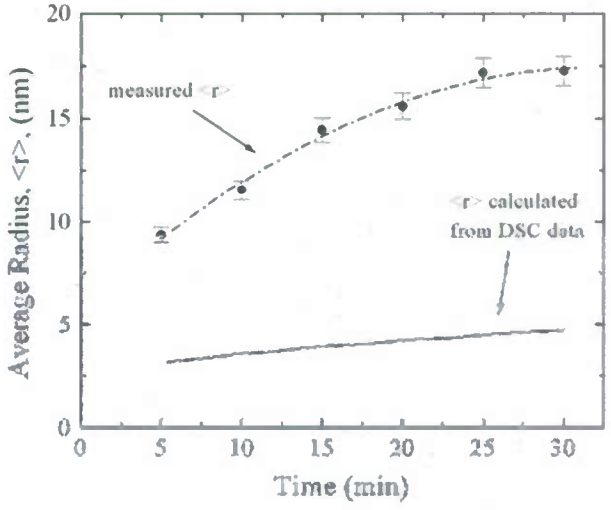

Figure 4 - Measured average radius (circles) and that calculated from eq. (3). The dash-dot line is a guide to the eye.

These studies indicate that rapidly-quenched $Al_{88}Y_7Fe_5$ alloys are indeed glasses. The appearance of coarsening arises from the extremely rapid nucleation, followed by diffusion-limited growth. They demonstrate that DSC isothermal measurements do not provide a "litmus-test" for distinguishing amorphous from nanocrystalline structures, as has been previously argued [49, 50].

B. Influence of Microalloying on Nucleation and Growth

As shown in Fig. 2.b, a nucleation and growth DSC peak, indicating the glassy nature of the alloy, arises with the substitution of only 0.5 at.% Ti for Al, (Fig. 1.a) [7]. Our previous studies demonstrated that the Ti does not act as an oxygen scavenger [7], but either raises the nucleation barrier for α-Al, slows the kinetics, or influences both processes. We also demonstrated that the addition of V led to a glass with the largest supercooled liquid region of any Al-based glass [8] Over the course of this contract, we have made a survey of the microalloying behavior of different 3d transition metals (TM) as microadditions [55]. In all cases the substitution of 0.5 at.% Al by the TM increases the crystallization temperature. However, as is shown in Fig. 5, the devitrification pathway changes depending on the TM microaddition. All alloys show a series of two to five exothermic peaks in the DSC nonisothermal scans. The two most prominent peaks in the glasses made with the microaddition of the middle transition metals (Fe and Mn) are sharp and symmetric, typical for the formation of intermetallic compounds. The other

alloys, in contrast, exhibit a series of broader peaks; the primary devitrification peak is particularly broad and in most compositions overlaps with a second peak.

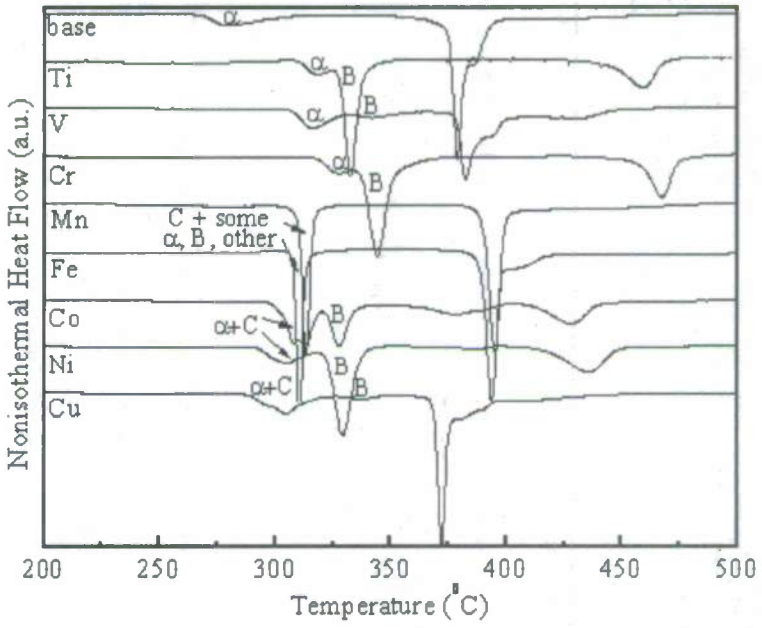

Figure 5 - Nonisothermal DSC scans (20 °C/min) of $Al_{87.5}Y_7Fe_5TM_{0.5}$. Primary crystallizing phases are identified as: α = α-Al, B = metastable B and C = metastable C phases.

The broad primary devitrification DSC peak for the alloys made with microadditions of the early transition metals (Ti, V, Cr) corresponds to the formation of α-Al. The second peak with an onset at 15-25 °C higher temperature, but overlapping with the first peak, is due to the formation of a metastable intermetallic phase(B). In contrast, the late transition metal microalloys (Co, Ni, Cu) concurrently form both α-Al and a different metastable phase (C), followed by a well-separated DSC peak corresponding to the formation of phase B. Finally, the sharp primary crystallization DSC peak for the alloys microalloyed with the middle transition metals, Mn and Fe, is due to crystallization to several phases, including the metastable B and C phases and a small amount of α-Al. In contrast, the primary devitrification of $Al_{88}Y_7Fe_5$ is to α-Al at a significantly lower temperature than primary devitrification of all of the alloys containing the microaddition; no evidence for metastable phase formation was observed. All alloys ultimately devitrify to the same assortment of α-Al, Al_3Y, and AlYFe phases. The structures of the metastable phases may contain clues about changes in the glass structure. Their nanoscale sizes make structural determination very difficult, however; we were unable to obtain any significant structural information even from tilting or high resolution TEM studies.

An examination of the partially devitrified samples shows that the crystal grains in the samples made with Ti are much more dendritic than in those made without the microaddition (Fig. 6). This indicates that the rejection of Y and Fe during crystallization to α-Al is more difficult in the alloys made with the microadditions.

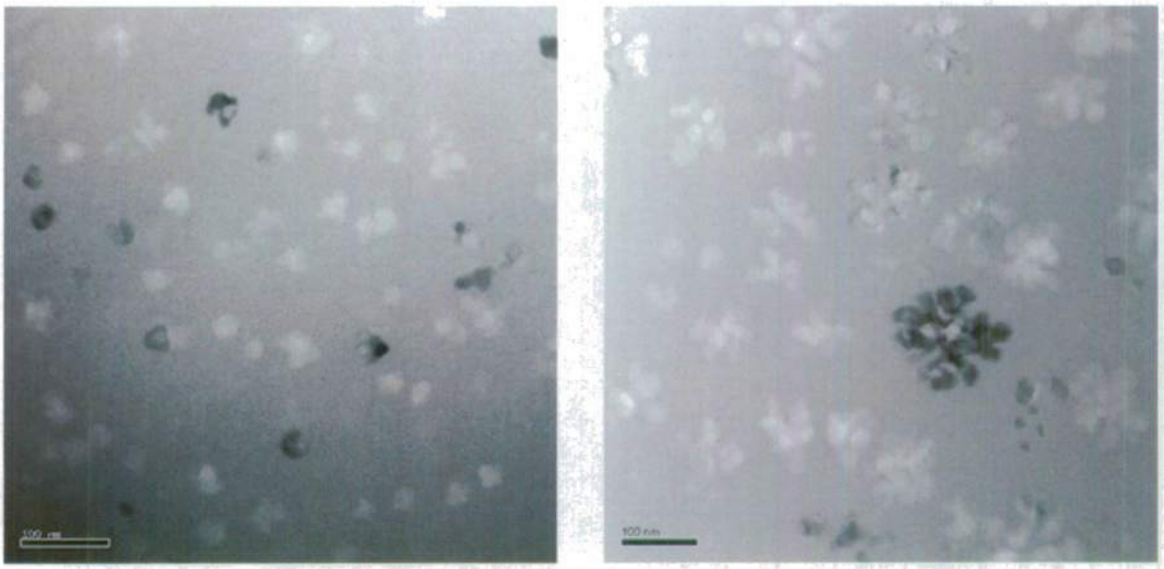

Figure 6 - Bright field TEM images of partially devitrified rapidly quenched samples. Left – $Al_{88}Y_7Fe_5$ after annealing at 250°C for 30 minutes. Right – $Al_{87.5}Y_7Fe_5Ti_{0.5}$ after annealing at 285°C for 30 minutes.

It was planned to measure the particle size distributions in alloys made with and without the microadditions, and to compare these with calculations from the coupled flux model for nucleation and growth that we have developed. However, the strongly dendritic character of the grains made it difficult to accurately identify the grain edges, introducing a considerable error in the size determination. It was still useful, however, to measure the saturation particle density (Fig. 7).

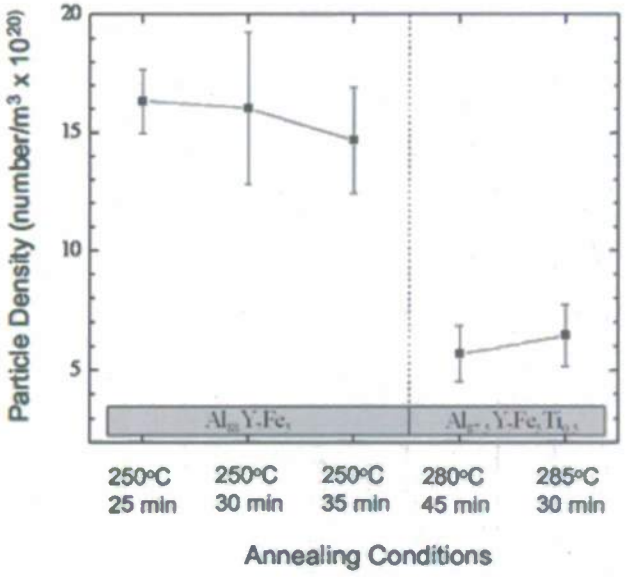

Figure 7 - Saturation density of particles in $Al_{88}Y_7Fe_5$ and $Al_{87.5}Y_7Fe_5Ti_{0.5}$ for a range of annealing conditions. Error bars indicate the standard deviation in the measurements.

These data show that the number of particles is approximately constant for the same alloy under a range of annealing conditions. It is larger in the glass made without Ti, suggesting that as for the resistivity results that are discussed in the next section, the transformation kinetics reflect a structure in the glass. The 3DAP studies carried out under NSF support show that this is due to a nanoscale phase separation into regions of nearly pure Al in the glasses made without the microaddition.

C. Electrical Resistivity Studies of Devitrification

Measurements of the electrical resistivity support the conclusion that the rapidly-quenched base alloy ($Al_{88}Y_7Fe_5$) is amorphous and that the addition of Ti changes the transformation kinetics. Figure 8.a shows the resistance change with the crystallization of $Al_{88}Y_7Fe_5$ as a function of annealing time.

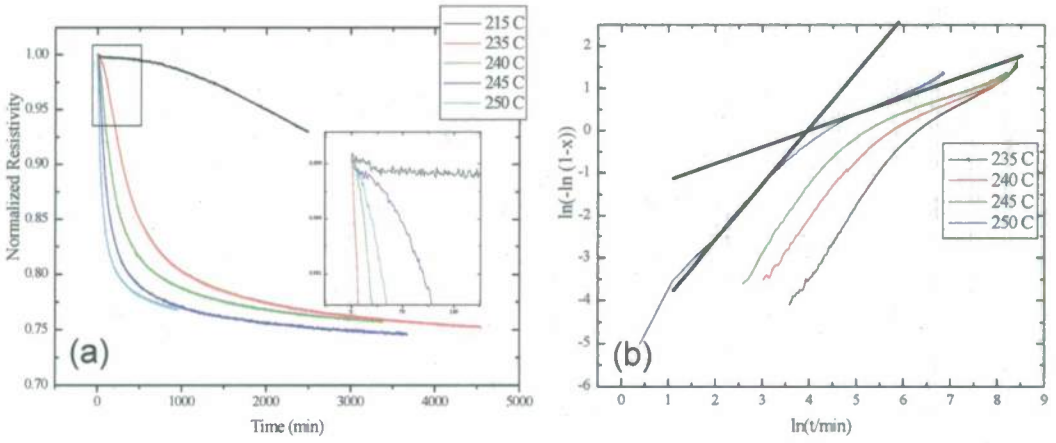

Figure 8 – (a) Measurements on rapidly-quenched samples of $Al_{88}Y_7Fe_5$ of the resistivity normalized to the initial resistivity as a function of annealing time at different temperatures. No sigmoidal behavior is observed for temperatures above 235°C (see inset). (b) Johnson-Mehl-Avrami-Kolmogorov plot of the volume fraction transformed as a function of annealing time.

For high temperatures, the short-time behavior of the change is not resolvable due to the temperature equilibrium time (analogous to the instrumental transient in the DSC data). However, because measurements can be extended to lower temperatures than the DSC measurements, the initial character of the transformation can be resolved. A sigmoidal character of the resistivity change upon anneal is observed (see inset), indicative of nucleation and growth based crystallization.

The extremely high initial nucleation rates and the overlapping diffusion fields from the grains (soft impingement) make the calculation of the volume fraction transformed extremely difficult. Computer modeling is required for a quantitative analysis. To gain qualitative insight, the data in Fig. 8.b were analyzed using the JMAK [56] analysis, assuming that the volume fraction transformed, x, scaled linearly with the change in electrical resistivity

$$x = 1 - \exp\left(-K'(T)t\right)^n . \quad (6)$$

Here *K'(T)* is a temperature-dependent parameter that characterizes the effective kinetics of the transformation (it is different from the kinetic factor in eq. (4)) and *n* is the Avrami coefficient, which provides some insight into the transformation mechanism. From eq. (6),

$$\ln\left[\ln(1-x)^{-1}\right] = n\ln K'(T) + n\ln t . \quad (7)$$

A plot of $\ln\left[\ln(1-x)^{-1}\right]$ *vs* $\ln t$ should then produce a straight line with slope *n* and intercept *n* ln *K'(T)*. Fig. 8.b shows a plot of eq. (7) for the electrical resistivity data as a function of annealing for rapidly-quenched $Al_{88}Y_7Fe_5$ alloys. The values for the Avrami coefficients are listed as a function of annealing temperature in Table I. A range of values for *n* between 1.14 and 1.62 are found in the earliest stages of the transformation, with the value decreasing with increasing annealing temperature. A rather sharp transition to much lower values ($0.54 \leq n \leq 0.67$) is observed at very nearly the same volume fraction transformed ($x \approx 0.57$). Again, the value of the Avrami coefficient decreases with increasing annealing temperature). The appearance of a transition at approximately the same value for all annealing temperatures suggests that it is linked to the microstructure of the initial glass.

Table I
Avrami Coefficients (Eq. 7) for crystallization of $Al_{88}Y_7Fe_5$

Annealing Temperature (°C)	Initial Value of n	Final Value of n	Volume Fraction at Knee
235	1.62	0.67	0.56
240	1.31	0.54	0.57
245	1.46	0.48	0.56
250	1.14	0.54	0.57

The crystallization kinetics for the $Al_{87.5}Y_7Fe_5Ti_{0.5}$ glass are slower than for the $Al_{88}Y_7Fe_5$ samples at the same temperature, supporting the DSC data that show that microalloying improves glass stability. The electrical resistivity results are shown in Fig. 9 and the results of the JMAK analysis are listed in Table II.

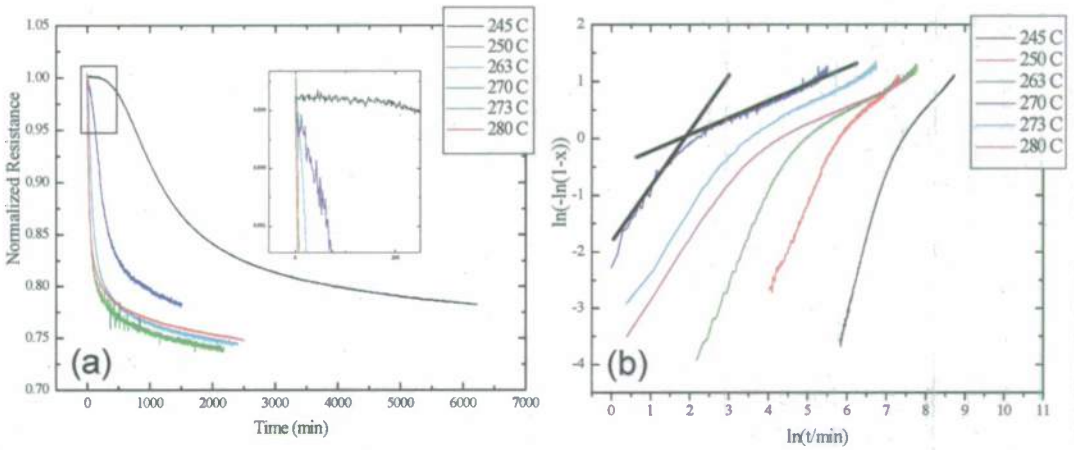

Figure 9 – (a) Measurements on rapidly-quenched samples of $Al_{88}Y_7Fe_5$ of the resistivity normalized to the initial resistivity as a function of annealing time at different temperatures. No sigmoidal behavior is observed for temperatures above 235°C (see inset). (b) Johnson-Mehl-Avrami-Kolmogorov plot of the volume fraction transformed as a function of annealing time.

Table II
Avrami Coefficients (Eq. 7) for crystallization of $Al_{87.5}Y_7Fe_5Ti_{0.5}$

Annealing Temperature (°C)	Initial Value of n	Final Value of n	Volume Fraction at Knee
245	2.35	0.86	0.56
250	1.73	0.69	0.61
263	1.58	0.42	0.58
270	1.09	0.30	0.62
273	1.09	0.43	0.55
280	0.91	0.28	0.59

A larger range of values for n, between 0.91 and 2.35, are found in the earliest stages of the transformation, with the value decreasing with increasing annealing temperature. Again a rather sharp transition to much lower values ($0.28 \leq n \leq 0.86$) is observed at very nearly the same volume fraction transformed ($x \approx 0.6$) as for the glass containing no Ti. The value of the Avrami coefficient again decreases with increasing annealing temperature, but the change is over a much larger range. The small n values at the end of the transformation is strongly suggestive of diffusion-limited growth with strong soft-impingement. The nearly same volume fraction in the two glasses for the change in slope indicates that soft-impingement becomes dominant at about the same stage in the transformation process.

D. Fluctuation Electron Microscopy

Our work has demonstrated that when the coherence length of order in the glass becomes of the same magnitude as the critical size for nucleation, it can couple strongly to the

nucleation barrier. A natural question, then, is does the microalloying change the medium range order in the glass? Only recently, with the development of a transmission electron microscopy technique called fluctuation electron microscopy (FEM), has it become possible to measure such medium-range order (MRO) in amorphous materials [57]. Fluctuations in hollow cone dark-field images are analyzed over a range of incident illumination directions, q. These fluctuations, quantitatively represented by the calculated variance contain information of higher order correlations, the three- and four-body correlations as well as the two -body correlations that contribute to $S(q)$.

A variant of this technique, which uses a scanning probe, is called Scanning Probe (SP-FEM, sometimes also termed STEM-FEM) [58]. In SP-FEM, nanodiffraction patterns are recorded using a focused nanometer-sized probe at different locations of a specimen within an $n \times n$ spatial grid. SP-FEM allows a denser sampling in scattering vector at a lower dose than the TEM technique. The higher density of data is useful for obtaining more precise information on three- and four-body correlations and the lower sample dose reduces changes in the signal due to sample contamination during the measurements. Also, the STEM technique can easily allow data to be automatically collected for different probe sizes by systematically changing the excitation of the lenses forming the probe size; in the TEM method, one must change the objective aperture by hand. A fluctuation map could, therefore, be more easily constructed by varying both the scattering vector, k, (variable coherence microscopy) and the aperture size (variable resolution microscopy), yielding better information on the high-order correlations and additional constraints for potential models.

Supported jointly by this AFOSR contact, our NSF grant and internal funding, we have implemented SP-FEM on the Jeol 2100 FX located in the CMI at Washington University. In this technique, a small (1-2 nm) coherent electron probe is scanned over a 10x10 grid of spatial locations that are spaced 2 nm apart to obtain 100 local diffraction patterns. From these data, the variance in the diffraction intensities is calculated. We have developed several approaches to compute this variance. Two that are discussed in this report are:

- Annular-mean variance (V_Ω) – the annular mean intensity for a diffraction ring of radius k (reciprocal lattice) is computed for each of the 100 diffraction patterns is computed ($\Omega_i(k)$ and the variance is computed from

$$V_\Omega = \frac{\left\langle \Omega_i^2(k) \right\rangle}{\left\langle \Omega_i(k) \right\rangle^2} - 1,$$

  where < > indicates the average.
- Annular mean of image variance $\Omega(V_{NBD})$ – the annular mean of the variance (calculated as the variance of each n-member set of intensities corresponding to each pixel location in the individual 100 diffraction patterns).

Our studies demonstrate that the FEM technique is very sensitive to experimental parameters such as sample preparation, which must be done by electrolytic thinning since ion milling causes structure changes near the surface due to implantation damage. Variance in the diffracted intensity is not only a function of MRO, but also a function of experimental parameters such as sample thickness, where slight variations can obscure features arising from the MRO. This strong influence of thickness is rarely discussed in the literature and when discussed it is inadequately characterized or considered. Our results clearly demonstrate that a constant sample thickness for the FEM measurements is extremely important for meaningful comparative results. The mean thickness of the specimen in the *n x n* raster field was measured using electron energy loss spectroscopy. Only those raster regions that fall with a tight range of mean thickness (0.7 ± 0.1 mean free electron paths) were measured and compared. We investigated the influence of probe focus (condenser lens setting) on the SP-FEM variance and observed that small changes from probe crossover at the specimen can influence the SP-FEM variance. We have also developed techniques that allow us to reproducibly set the probe focus for measurements.

Figures 10 and 11 shows the AP-FEM data for $Al_{88}Y_7Fe_5$ rapidly quenched alloys, made with and without the Ti microadditions. Both the annular-mean variance (V_Ω) and the image variance ($\Omega(V_{NBD})$) decrease when 0.5% of the Al is replaced by Ti, Mn or Ni, although the change in $\Omega(V_{NBD})$ is significantly less.

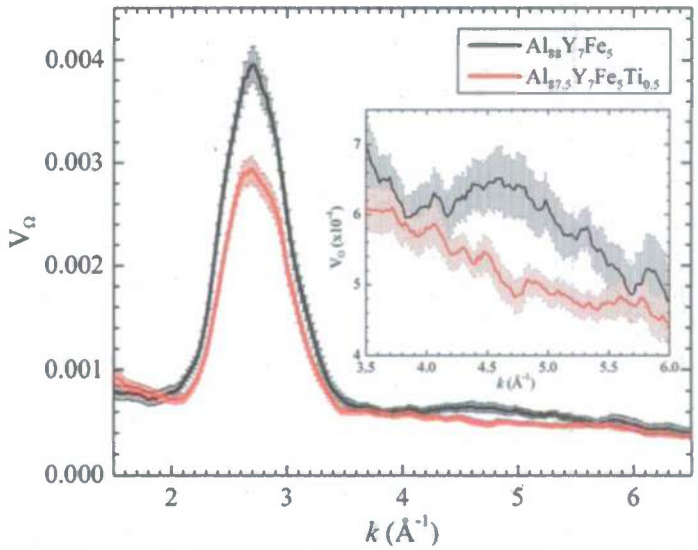

Figure 10 – Annular mean variance for representative samples in the $Al_{88}Y_7Fe_5$ and $Al_{87.5}Y_7Fe_5Ti_{0.5}$ alloys. Error bars indicate the standard error.

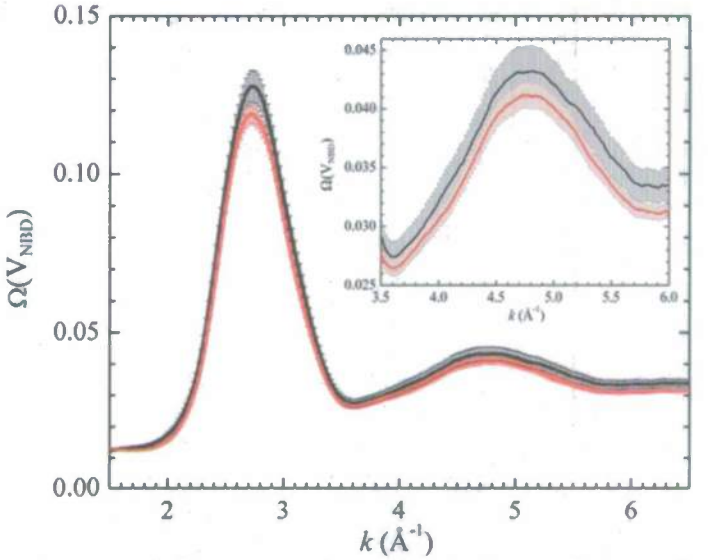

Figure 11 - Annular mean of image variance for in the $Al_{88}Y_7Fe_5$ and $Al_{87.5}Y_7Fe_5Ti_{0.5}$ alloys. Error bars indicate the standard error.

These results demonstrate that the medium-range order of the glass is changed with the introduction of transition metal microadditions. By acquiring data as a function of probe size, the size of the MRO could be estimate at 1.3 nm, which corresponds closely with a that expected for a pre-peak (indicating intermediate range ordering) observed in our synchrotron x-ray diffraction studies.

V. Conclusions

We have demonstrated that rapidly-quenched $Al_{88}Y_7Fe_5$ alloys are indeed amorphous, even though they do not show a visible glass transition and their transformation behavior in isothermal differential scanning calorimetry experiments is more consistent with coarsening. Their transformation is dominated by an extremely rapid nucleation rate, followed by very slow diffusion-limited growth, likely due to rejection of the Y. As proposed, we have investigated the reasons that Ti microadditions might improve glass formability and stability, whether other transition metal microadditions might work as well or better. Calorimetric and microstructural studies indicate that these microadditions both raise the nucleation barrier for the α-Al phase and increase the role of long-range diffusion. An examination with a new technique, scanning probe fluctuation electron microscopy (SP-FEM), of samples made with and without Ti microaddition show that the Ti microaddition induces a change in the medium range order. The variance in samples made with Ti is lower than in the sample without Ti. Since the variance will be zero for both a completely disordered sample, or a perfectly ordered one (such as a crystal), it is unclear from SP-FEM measurements alone whether the Ti increases or decreases the disorder.

Additional Insight from NSF-DMR-0606065 - Recent studies that were supported by my NSF grant (DMR-0606065) have provided valuable information that allows a deeper

interpretation of the results obtained with AFOSR support [59]. We have made three dimensional atom probe tomography (3DAP) measurements on samples with and without Ti. The $Al_{88}Y_7Fe_5$ samples show a high density (approximately $10^{25}/m^3$) of pure Al zones, some containing up to 50 atoms. The Y and Fe solute atoms appear to be largely excluded from these regions. A longer-range chemical fluctuation was also observed, showing a separation between Al-rich (91 at.%) and Al-depleted (82 at.%). The separation is not random, but follows a sinusoidal pattern, strongly suggesting phase separation for a Cahn-Hilliard type mechanism for phase separation on a length scale of approximately 100 nm. The density of the regions of maximum Al concentration (91 at.% Al) is similar to that of the crystallite densities (10^{21}-10^{23} m^{-3}) in the crystallized alloy. The pure-Al zones in Al-rich regions likely are the sites for the rapid nucleation of α-Al, since the nucleation barrier would be very small, explaining the rapid production of a high density of α-Al grains. The surrounding regions containing higher concentrations of Fe and Y would slow diffusion, explaining the slow grain growth. Atom probe studies of as-quenched $Al_{87-x}Y_7Fe_5Ti_x$ glasses do not show evidence for the phase separation, indicating that it is suppressed by the microaddition of Ti. This explains why these glasses are more stable and show normal nucleation and growth behavior. These observations also allow an interpretation of the SP-FEM results. The decreased variance observed for the $Al_{87-x}Y_7Fe_5Ti_x$ reflects the increased chemical homogeneity.

The tendency for many Al-based metallic glasses to crystallize to an a nanocrystal/glass composite and the recently reported evidence for phase separation in a related glasses ($Al_{89}Ni_6La_5$) [60] raises the question of whether nanoscale phase separation is common in Al-based glasses. If so, it is unlikely that these glasses can be made into bulk metallic glasses.

VI. Acknowledgement/Disclaimer

This work was sponsored (in part) by the Air Force Office of Scientific Research, USAF, under grant/contract number FA 9550-05-1-0110. The views and conclusions contained herein are those of the authors and should not be interpreted as necessarily representing the official policies or endorsements, either expressed or implied, of the Air Force Office of Scientific Research or the U.S. Government.

The personnel and travel costs for the 3DAP and synchrotron studies were supported by the National Science Foundation (DMR-0606065). The APT data were obtained at Oak Ridge National Laboratory using the SHaRE User Facility that was sponsored by Basic Energy Sciences, U.S. Department of Energy. The synchrotron measurements were made on the MUCAT beam-line at the Advanced Photon Source. Work in the MUCAT Sector at the APS, and the Ames Laboratory was supported by the Department of Energy, Basic Energy Sciences, under Contract No. DS-AC02-07CH11358. Use of the Advanced Photon Source was supported by the U. S. Department of Energy, Office of Science, Office of Basic Energy Sciences, under Contract No. DE-AC02-06CH11357.

VII. Products and Support

Personnel supported under this grant

Kenneth F. Kelton	Professor, Washington University, St. Louis, MO
William E. Buhro	Professor, Washington University, St. Louis, MO
Anindita Mukhopadhyay	Postdoctoral Assoc., Washington University, St. Louis, MO
Anup K. Gangopadhyay	Postdoctoral Assoc., Washington University, St. Louis, MO
Karyn Spence Bondi	Graduate Student, Washington University, St. Louis, MO
Debajit Saha	Graduate Student, Washington University, St. Louis, MO

PhD Thesis

One PhD thesis entitled, "Analysis of the effects of microalloying on glass formation in Al-Y-Fe alloys by fluctuation electron microscopy and other techniques," has been written on Karyn Spence Bondi on research partially supported by the AFOSR grant. She will defend her thesis on April 9, 2009. After successful completion of the PhD requirements, her thesis will be microfilmed and available at ProQuest (UMI Dissertation Publishing) http://www.proquest.com/en-US/products/dissertations/.

Publications

1. "Liquid Structure and Long Range Diffusion – Their Impact on Glass Formation and Nanoscale Devitrification," K. F. Kelton, Intermetallics, **14**, 966 (2006).
2. "Intermediate-range order in amorphous metal alloys," P. C. Gibbons, Y. T. Shen, K. Spence, L.-Q. Xing and K. F. Kelton, Phil. Mag., **86**, 293 (2006).
3. "Influence of Microalloying on Glass Formation and Crystallization," K. F. Kelton, J. Alloys and Compounds, **434-435**, 115 (2007).
4. "An Al-rich metallic glass with a large supercooled liquid region," A. Mukhopadhyay, K. E. Spence, L. Q. Xing, W.E. Buhro, K. F. Kelton, Phil. Mag., **87**, 281 (2007).
5. "Structural Aspects of Metallic Glasses," D. B. Miracle, T. Egami, K. F. Kelton and K. M. Flores, MRS Bulletin **32**, 629 (2007).
6. "Local order and nanostructure induced by microalloying in Al–Y–Fe amorphous alloys," A. Sadoc, O. Heckmann, V. Nassif, O. Proux, J.-L. Hazemann, L.Q. Xing and K.F. Kelton, J. Non-Crystalline Solids, **353**, 2758 (2007).
7. "Effects of microalloying with 3d transition metals on glass formation," K. S. Bondi, A. K. Gangopadhyay, Z. Marine, T. H. Kim, A. Mukhopadhyay, A. I. Goldman, W. E. Buhro, K. F. Kelton, J. Non-Cryst. Solids, **353**, 4723 (2007).

Invited Lectures

1. "Amorphous Metal Formation and Crystallization - Coupled Processes in Crystal Nucleation," K. F. Kelton, Oak Ridge National Laboratory, High Temperature Materials Laboratory, Oct. 28, 2005.
2. "Influence of Local Structure and Alloy Composition on Glass Formation and Stability," Hume-Rothery Symposium: The Science of Complex Alloys, TMS Meeting, San Francisco, CA, Feb. 13-17, 2005.

3. "Coupled Processes in Nucleation," Frontiers in Solidification Science, Nucleation, TMS Meeting, San Francisco, CA, Feb. 13-17, 2005.
4. "The Importance of Local Structure and Chemistry on Glass Formation and Crystallization", K. F. Kelton, Solid-State Phase Transformations in Inorganic Materials (PTM 2005), May 29 – June 3, 2005.
5. "Glass Formation and Microalloying," K. F. Kelton, ISMANAM 2005, Paris, France, 4-7 July, 2005.
6. "Amorphous Metal Formation and Crystallization-Coupled Processes in Crystal Nucleation," K. F. Kelton, University of Illinois, Urbana-Champaign, IL, May 1, 2006.
7. "Amorphous Metal Formation and Crystallization- Coupled Processes in Crystal Nucleation," K. F. Kelton, Hanyang University, Seoul, Korea, May 11, 2006.
8. "The Importance of Local Structure and Chemistry on Glass Formation and Crystallization," K. F. Kelton, Yonsei University, Seoul, Korea, May 12, 2006.
9. "Coupled Kinetic and Order Parameter Processes in Nucleation," K. F. Kelton, Nucleation Symposium, 80th ACS Colloid and Surface Science Symposium, Boulder Colorado, June 18-21 2006.
10. "Role of Coupled Nucleation Processes in Amorphous Metal Formation and Nano-Crystallization," K. F. Kelton, Workshop – Critical Issues and Future Directions in Solidification Science, Iowa State University, Ames, IA, September 20-22,
11. "The Importance of Coupled Nucleation and Micro-alloying for Metallic Glass Formation and Crystallization," K. F. Kelton, 8th International Symposium on Crystallization in Glasses and Liquids, Jackson Hole, Wyoming, September 24-28, 2006.
12. "Role of Coupled Nucleation in Metallic Glass Formation and Nanocrystallization," K. F. Kelton, University of Missouri, Rolla, MO, October 12, 2006.
13. "Coupled Order Parameter Nucleation Processes in Metallic Glasses," K. F. Kelton, Bulk Metallic Glass Symposium, TMS 2007 Annual Meeting, Orlando, FL, Feb. 25-Mar. 1, 2007.
14. "Coupled Nucleation Processes and Glass Crystallization," K. F. Kelton, Symposium on Atom Probe Tomography: Opportunities and Challenges for New Materials Science, Iowa State University, Ames IA, May 30, 2007.
15. "Transition Metal Microadditions and Glass Formation in Rapidly-Quenched $Al_{88}Y_7Fe_5$ Alloys," TMS Annual Meeting, New Orleans, LA, March 9-13, 2008.

References

1. Y. He, S. J. Poon, and G. J. Shiflet, *Science*, **241,** 1640 (1988).
2. A. Inoue, *Prog. Mater. Sci.*, **43,** 365 (1998).
3. Y. Kawamura, H. Mano, and A. Inoue, *Scripta Matall. Mater.*, **44,** 1599 (2001).
4. M. E. Goldman, N. Unlu, G. J. Shiflet, and J. R. Scully, *Electrochemical and Solid State Lett.* , **8,** B1 (2005).
5. A. L. Greer, *Nanostructured Mater.*, **50,** 143 (1998).
6. A. L. Greer, *Mat. Sci. and Eng.*, **A304-306,** 68 (2001).
7. L. Q. Xing, A. Mukhopadhyay, W. E. Buhro, and K. F. Kelton, *Phil. Mag. Lett.*, **84,** 293 (2004).
8. A. Mukhopadhyay, S. K. E., L. Q. Xing, W. E. Buhro, and K. F. Kelton, *Phil. Mag.*, **87,** 281 (2007).
9. A. Inoue, K. Ohtera, A. P. Tasi, and T. Masumoto, *Jpn. J. Appl. Phys.*, **27,** L280 (1988).
10. A. Inoue, K. Ohtera, K. Kita, and T. Masumoto, *Jpn. J. Appl. Phys.*, **27,** L736 (1988).
11. Y. He, S. J. Poon, G. J. Shiflet, *Science*, **241,** 1640 (1988).
12. T. Egami and Y. Waseda, *J. Non-Cryst. Solids*, **64,** 113 (1984).
13. O. N. Senkov and D. B. Miracle, *Mater. Res. Bull.* , **36,** 2183 (2001).
14. T. Egami, *J. Non-Cryst. Solids*, **317,** 30 (2003).
15. S. J. Poon, G. J. Shiflet, F. Q. Guo, and V. Ponnambalam, *J. Non-Cryst. Solids*, **317,** 1 (2003).
16. D. B. Miracle, *Nature Mater.*, **3,** 697 (2004).
17. M. Calin and U. Koester, *Mater. Sci. Forum*, **269-272,** 749 (1998).
18. S. K. Das, J. H. Perepezko, R. I. Wu, and G. Wilde, *Mat. Sci. and Eng. A*, **304-306,** 159 (2001).
19. A. P. Tsai, T. Kamiyama, Y. Kawamura, A. Inoue, and T. Masumoto, *Acta Mater.*, **45,** 1477 (1997).
20. K. F. Kelton and A. L. Greer, *J. Non-Cryst Solids*, **79,** (1986).
21. A. Inoue, C. Fan, J. Saida, and T. Zhang, *Sci. Tech. Adv. Mater.*, **1,** 73 (2000).
22. S. Atanassova, K. Neykov, and I. Gutzow, *J. Cryst. Growth*, **212,** 233 (2000).
23. E. Belin-Ferre, R. G. Hennig, Z. Dankhazi, A. Sadoc, J. Y. Kim, and K. F. Kelton, *J. Alloys & Comp.*, **342,** 337 (2002).
24. Y. Yoshizawa and K. Yamauchi, *Mater. Trans. JIM*, **31,** 307 (1990).
25. R. Busch, S. Schneider, A. Peker, and W. L. Johnson, *Appl. Phys. Lett.*, **67,** 1544 (1995).
26. R. Busch, S. Schneider, A. Peker, and W. L. Johnson, *Appl. Phys. Lett.*, **67,** 1544 (1995).
27. K. F. Kelton, T. K. Croat, A. K. Gangopadhyay, L. Q. Xing, A. L. Greer, M. Weyland, X. Li, and K. Rajan, *J. Non-Cryst. Solids*, **317,** 71 (2003).
28. K. Hono, K. Hiraga, Q. Wang, A. Inoue, and T. Sakurai, *Acta Metall. et Mater.*, **40,** 2137 (1992).
29. M. Ohnuma, K. Hono, S. Linderoth, J. S. Pedersen, Y. Yoshizawa, and H. Onodera, *Acta Mater.*, **48,** 4783 (2000).
30. K. F. Kelton, *Acta Mater.*, **48,** 1967 (2000).

31. K. F. Kelton, *Phil. Mag. Lett.*, **77,** 337 (1998).
32. K. F. Kelton, G. W. Lee, A. K. Gangopadhyay, R. W. Hyers, T. Rathz, J. Rogers, M. B. Robinson, and D. Robinson, *Phys. Rev. Lett.*, **90,** 195504 (2003).
33. P. J. Desre, E. Cini, and B. Vinet, *J. Non-Cryst. Solids*, **288,** 210 (2001).
34. F. C. Frank, *Proc. Royal Soc. London*, **215A,** 43 (1952).
35. B. Zhang, D. Q. Zhao, M. X. Pan, R. J. Wang, and W. H. Wang, *Acta Mater.*, **54,** 3025 (2006).
36. L. He and J. Sun, *Scripta Mater.*, **54,** 1081 (2006).
37. B. Liu, L. Liu, M. Sun, C. L. Qiu, and Q. Chen, *Acta Metall. Sinica*, **41,** 738 (2005).
38. B. Liu and L. Liu, *Mat. Sci. Eng.*, A**415,** 286 (2006).
39. C. Y. Luo, Y. H. Zhao, X. K. Xi, G. Wang, D. Q. Zhao, M. X. Pan, W. H. Wang, and S. Z. Kou, *J. Non-Cryst. Solids*, **352,** 185 (2006).
40. Z. P. Lu and C. T. Liu, *J. Mater. Sci.*, **39,** 3965 (2004).
41. C. T. Liu and Z. P. Lu, *Intermetallics*, **13,** 415 (2005).
42. J. Eckert, N. Mattern, M. Zinkevitch, and M. Seidel, *Mater. Trans., JIM*, **39,** 623 (1998).
43. B. S. Murty and D. H. Ping, *Mat. Sci. Eng.*, **A304-A306**, 706 (2001).
44. A. Inoue, *Mater. Trans., JIM*, **40,** 1181 (1999).
45. J. Saida, *J. Phys.: Cond. Matter*, **13,** L73 (2001).
46. L. Q. Xing, T. C. Hufnagel, J. Eckert, W. Loser, and L. Schultz, *Appl. Phys. Lett.*, **77,** 1970 (2000).
47. L. Q. Xing, Y. T. Shen, and K. F. Kelton, *Appl. Phys. Lett.*, **81,** 3371 (2002).
48. K. F. Kelton and J. C. Holzer, *Rev. Sci. Instrum.*, **59,** 347 (1988).
49. L. C. Chen and F. Spaepen, *J. Appl. Phys.*, **69,** 679 (1991).
50. L. C. Chen and F. Spaepen, *Mat. Sci. Eng.*, **A133**, 342 (1991).
51. K. F. Kelton, *J. Non-Cryst. Solids*, **274** 147 (2000).
52. K. F. Kelton, *J. Alloys and Comp.*, **434-435,** 115 (2007).
53. I. M. Lifshitz and V. V. Slyozov, *Phys. Chem. Solids*, **19,** 35 (1961).
54. C. Wagner, *Z. Elektrochem.*, **65,** 581 (1961).
55. K. S. Bondi, A. K. Gangopadhyay, Z. Marine, T. H. Kim, A. Mukhopadhyay, A. I. Goldman, W. E. Buhro, and K. F. Kelton, *J. Non-Cryst. Solids*, **353,** 7233 (2007).
56. J. W. Christian, *The Theory of Transformations in Metals and Alloys*. 2nd ed. 1975, Oxford: Pergamon Press.
57. M. M. J. Treacy, J. M. Gibson, L. Fan, D. J. Paterson, and I. McNutty, *Rep. Prog. Phys.*, **68,** 2899 (2005).
58. P. M. Voyles and D. A. Muller, *Ultramicroscopy*, **93,** 147 (2002).
59. K. K. Sahu, N. A. Mauro, L. Longstreth-Spoor, Z. Nussinov, M. K. Miller, and K. F. Kelton, (private communication).
60. B. Radiguet, D. Blavette, N. Wanderka, J. Banhart, and K. L. Sahoo, *Appl. Phys. Lett.*, **92,** 103126 (2008).